LA-UR-17-26003 (Accepted Manuscript)

Superposition Principle in Auger Recombination of Charged and Neutral Multicarrier States in Semiconductor Quantum Dots

Wu, Kaifeng
Lim, Jaehoon
Klimov, Victor Ivanovich

To be published in: ACS Nano

DOI to publisher's version: 10.1021/acsnano.7b04079

Permalink to record: http://permalink.lanl.gov/object/view?what=info:lanl-repo/lareport/LA-UR-17-26003

Superposition Principle in Auger Recombination of Charged and Neutral Multicarrier States in Semiconductor Quantum Dots

Kaifeng Wu[1,2], Jaehoon Lim[1], and Victor I. Klimov[1]*

[1]Chemistry Division, Los Alamos National Laboratory, Los Alamos, New Mexico 87545, USA

[2] State Key Laboratory of Molecular Reaction Dynamics and Collaborative Innovation, Dalian Institute of Chemical Physics, Chinese Academy of Sciences, 457 Zhongshan Road, Dalian 116023, China

*Address for correspondence: klimov@lanl.gov

Abstract

Application of colloidal semiconductor quantum dots (QDs) in optical and optoelectronic devices is often complicated by unintentional generation of extra charges, which opens fast nonradiative Auger recombination pathways whereby the recombination energy of an exciton is quickly transferred to the extra-carrier(s) and ultimately dissipated as heat. Previous studies of Auger recombination have primarily focused on neutral, and more recently, negatively charged multi-carrier states. Auger dynamics of positively charged species remains more poorly explored due to difficulties in creating, stabilizing, and detecting excess holes in the QDs. Here we apply photochemical doping to prepare both negatively and positively charged CdSe/CdS QDs with two distinct core/shell interfacial profiles ("sharp" *versus* "smooth"). Using neutral and charged QD samples we evaluate Auger lifetimes of biexcitons, negative and positive trions (an exciton with an extra electron or a hole, respectively), and multiply negatively charged excitons. Using these measurements, we demonstrate that Auger decay of both neutral and charged multi-carrier states can be presented as a superposition of independent *elementary* three-particle Auger events. As one of the manifestations of the *superposition principle*, we observe that biexciton Auger decay rate can be presented as a sum of the Auger rates for independent negative- and positive-trion pathways. By comparing the measurements on the QDs with the "sharp" *versus* "smooth" interfaces, we also find that while affecting the absolute values of Auger lifetimes, manipulation of the shape of the confinement potential does not lead to violation of the superposition principle which still allows us to accurately predict the biexciton Auger lifetimes based on the measured negative and positive trion dynamics. These findings indicate considerable robustness of the superposition principle as applied to Auger decay of charged and neutral multicarrier states, suggesting its generality to quantum-confined nanocrystals of arbitrary compositions and complexities.

Keywords: colloidal quantum dots, positively and negatively charged quantum dots, Auger recombination, multiexcitons, positive and negative trion

TOC Entry:

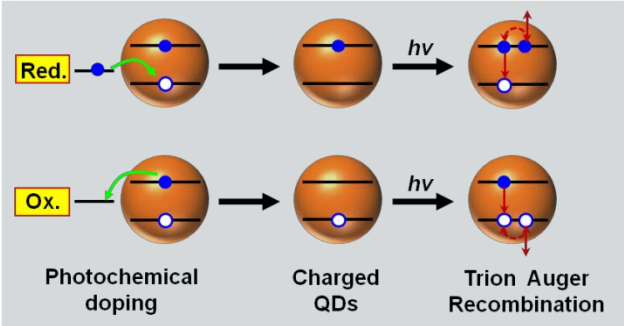

In well-passivated colloidal quantum dots (QDs), single electron-hole pair (single exciton) recombination is dominated by radiative decay. However, the presence of one or more extra-carriers triggers a highly efficient nonradiative Auger decay channel whereby the electron-hole recombination energy is released not as a photon but instead transferred to a third charge.[1, 2] Because of both confinement enhanced carrier-carrier interactions and the relaxation of momentum conservation, Auger decay in QDs is extremely fast (a few to hundreds of picoseconds)[2-5] which is detrimental to many prospective optical and optoelectronic applications of the QDs.

Auger recombination is especially harmful in the case of lasing applications, as optical gain directly relies on emission from multicarrier states.[6, 7] This process has been a primarily obstacle for the realization of stable continuous wave (cw) QD lasing as well as lasing with electrical pumping.[8, 9] Furthermore, recent studies of QD-based light emitting diodes (LEDs) indicate that imbalance between electron and hole injection currents can lead to QD charging which is accompanied by increasing carrier losses due to Auger recombination.[10, 11] This effect has been invoked as a possible reason for efficiency roll-off (a so-called “droop” effect)

typically observed for QD-LEDs for large driving currents.[10]

Previous studies have established several systematic trends in Auger recombination, which includes a linear dependence of Auger lifetimes on QD volume (sometimes referred to as a *V-scaling*)[2, 3] and a so-called *statistical scaling* of Auger decay rates (r_A) with per-dot numbers of electrons (N_e) and holes (N_h) comprising a given multicarrier state.[12, 13] Statistical scaling is a consequence of a more general *superposition principle* according to which the Auger decay rate of a given multicarrier state can be presented as a sum of Auger rates for all possible *elementary* three-particle Auger events.[12] Specifically, in the case when the rates of all elementary Auger events are the same and equal to $r_{0,A}$, the overall Auger recombination rate r_A of the (N_e,N_h)-state is proportional to the product of the total numbers of electron-hole recombination pathways (given by N_eN_h) and the energy transfer events (given by $N_e + N_h - 2$), and hence, can be calculated from $r_A = r_{0,A}N_eN_h(N_e + N_h - 2)$.[12] This situation can be realized in materials with mirror symmetric conduction and valence bands and highly degenerate band-edge states (the conditions satisfied in, *e.g.*, PbSe and PbS), when all carriers comprising a given multi-carrier state are virtually indistinguishable. In this model, the Auger decay rates of negative (X^-; $N_e = 2$ and $N_h = 1$) and positive (X^+; $N_e = 2$ and $N_h = 1$) trions are the same and equal to $r_{X-,A} = r_{X+,A} = 2r_{0,A}$. On the other hand, the biexciton (XX) Auger decay rate ($N_e = 2$ and $N_h = 2$) can be expressed as $r_A = 8r_{0,Ae}$ or $r_A = 2(r_{X-,A} + r_{X+,A})$. This suggests that biexciton decay can be thought of as occurring *via* two independent channels, one negative-trion and the other positive-trion like.

Experimental measurements of negatively charged excitons in PbSe QDs do indicate that the X^- Auger lifetime ($\tau_{A,X-}$) is approximately 4 times longer than that of the biexciton

($\tau_{A,XX}$),[13] as expected based on statistical scaling for materials with similar conduction- and valence-band electronic structures. According to conducted studies of negative trions in CdSe QDs, τ_{A,X^-} can be significantly longer than $4\tau_{A,XX}$.[14-16] Based on the superposition principle, this would imply a considerable asymmetry between negative (τ_{A,X^-}) and positive (τ_{A,X^+}) trion Auger pathways, with τ_{A,X^+} being much shorter than τ_{A,X^-}. The existence of such asymmetry was also indicated by recent single-dot measurements of CdSe-based core/shell structures that revealed two distinct low-emissivity states (assigned to X^- and X^+) with significantly different lifetimes ($\tau_{A,X^+} << \tau_{A,X^-}$).[17] The biexciton Auger lifetime inferred from the same measurements could be related to the time constants of the low-emissivity states by:

$$1/\tau_{A,XX} = 2(1/\tau_{A,X^+} + 1/\tau_{A,X^-}), \qquad (1)$$

which validated their assignment to oppositely charged trions.[17] This result also suggested the applicability of the superposition principle to the biexciton Auger decay rate even in the case of the significant asymmetry between the X^- and X^+ recombination pathways. However, this conclusion relied on measurements of single-dot emission in the presence of random charge fluctuations, when the number and even the sign of the fluctuating charges were poorly defined, while direct measurements of Auger recombination in QDs under conditions of controllable charging with both electrons and holes are still lacking.

In this work, we prepare both negatively and positively charged CdSe/CdS core/shell QDs using photochemical reduction or oxidation. Previously, this technique was successfully applied to generate negatively-charged QDs. [18] Here we extend this method to produce positively-charged samples containing extra holes. Since the applied methodology is based on scavenging one of the carriers of a photoinjected electron-hole pair (Scheme 1), it is

energetically much less challenging (by *ca.* a band gap energy) than QD charging *via* ground-state charge transfer.[13, 19] Thus, successful doping can be realized with relatively mild redox agents without degrading either the QD surface or the passivating layer, while this degradation represents a primary issue in the case of "ground-state" hole-doping of II-VI QDs.[20] Using negatively and positively charged QDs, we test the validity of the superposition principle and demonstrate, for example, that the biexciton Auger decay can indeed be presented as a superposition of independent negative and positive trion recombination pathways. We further use multiply-charged QDs to study scaling of Auger lifetimes with the number of extra electrons (up to $N_e = 5$), and again observe a close correspondence between the measurements and the predictions of the statistical model derived from the superposition principle. Finally, a side-by-side comparison between QDs with sharp and alloyed core/shell interfaces indicates that while "interface smoothing" leads to pronounced lengthening of Auger lifetimes it does not violate the superposition principle which still remains valid for both biexcitons and multiply charged single excitons.

Results/Discussion

Core/shell and core/alloy/shell QDs. In this work, we study two types of CdSe/CdS core/shell QDs with distinct properties of the core/shell interface. Both samples have the same (~3 nm) CdSe core diameter and the same (~9 nm) total diameter (see transmission electron microscopy, TEM, images in Figure 1a&b). However, one sample has a "sharp" core/shell interface (referred to as C/S QDs; Figure 1c) which is made possible by applying a fast-shelling synthesis reported in ref. 21. The other sample (referred to as C/A/S QDs; Figure

1d) has a graded core/shell interface comprised of three 0.5-nm-thick $CdSe_{1-x}S_x$ alloyed interlayers with x = 0.25, 0.5, and 0.75 (x increases from the inner to the outer layer); Figure 1d. Details of the synthesis can be found in the Methods and refs.[17, 21, 22]

According to previous theoretical studies,[23, 24] replacing a sharp step-like potential barrier (Figure 1c) with a smoother one (Figure 1d) can effectively suppress Auger recombination by reducing the probability of the intraband transition involved in dissipation of the electron-hole recombination energy. This prediction was confirmed by extensive studies of thick-shell "giant" CdSe/CdS QDs (g-QDs), where unintentional interfacial alloying was introduced during a fairly slow growth of the CdS shell by a successive ionic adsorption and reaction (SILAR) technique.[25, 26] More recently, the effect of suppression of Auger decay due to interface grading was investigated by intentionally introducing a thin $CdSe_{0.5}S_{0.5}$ alloy layer at the core/shell interface of the CdSe/CdS QDs.[22] Considerable benefits of this approach for LED and lasing applications of the QDs were discussed in refs. 9 and 10.

The absorption and photoluminescence (PL) spectra of C/S and C/A/S QDs are shown in Figure 1e. Despite the same size of the CdSe core, the 1S absorption and PL peaks of the C/A/S QDs (~660 nm) are red-shifted *versus* those of the C/S QDs (~630 nm) due to a stronger "leakage" of carrier wavefunctions outside the core. The PL quantum yields (QYs) of both types of QDs are ~50%. The single-exciton PL lifetime (Figure 1f), measured using time-correlated single photon counting (TCSPC), is slightly shorter for the C/A/S sample (~23 ns) than for the C/S sample (~29 ns). These ensemble lifetime constants are close to those observed for the "ON" states in single-dot measurements (not shown here), which

might suggest that the imperfect PL QYs of these samples arise from the existence of subsets of low-emissivity QDs with fast nonradiative recombination not resolvable in our measurements (the width of the instrument response function is ~200 ps).[21]

Neutral biexciton dynamics. To study recombination dynamics of neutral multiexciton in C/S and C/A/S samples, we monitor time resolved PL as a function of excitation fluence (Figure 2). In these measurements, samples were vigorously stirred to minimize effects due to uncontrolled photocharging.[27] With increasing pump photon fluence (j_p, quantified in terms of the number of photons per cm^2 per pulse), a fast decay component (sub-ns to ns time scales) emerges for both the C/A/S (Figure 2a) and the C/S (Figure 2d) QDs, which is a typical signature of multiexciton Auger recombination.[2, 28] The measured traces can be normalized such as to match their long-lived tails at times t > 10 ns where all multiexcitons have already decayed and PL relaxation is controlled by single-exciton recombination. At this stage, the signal magnitude (I_{long}) is proportional to the total number of photoexcited QDs, and hence, can be described as $I_{\text{long}} \propto (1 - p_0)$, where p_0 is the relative fraction of unexcited QDs in the ensemble. In the case of Poisson statistics of photon absorption events typically observed for QDs in the case of above band-gap excitation,[28] $p_0 = e^{-\langle N_{ph} \rangle}$, and hence, $I_{long} \propto 1 - e^{-\langle N_{ph} \rangle}$, where $\langle N_{ph} \rangle$ is the average number of photons absorbed per dot, per excitation pulse, which defines the average QD excitonic occupancy $\langle N \rangle$ immediately after photoexcitation. The latter quantity can be related to the photon per-pulse fluence by $\langle N \rangle = \sigma_{abs} j_p$, where σ_{abs} is the QD absorption cross-section at the pump photon energy (3.1 eV in our

measurements).

With σ_{abs} as the only adjustable parameter, we can perfectly fit the long-time PL signals for both the C/A/S (Figure 2b) and the C/S (Figure 2e) QD samples. The fitting procedure indicates that the absorption cross-sections are virtually the same for these two types of QDs ($\sigma_{abs} = 2\times10^{-14}$ cm^2), which is the consequence of similarity of their total volumes. The analysis of time-resolved PL signals also indicates that the initial PL intensity ($t = 0$) for the C/A/S QDs (Figure 2b) increases more rapidly with pump fluence than for the C/S QDs (Figure 2e). This reflects the difference in the Auger recombination rates in the two types of samples; specifically, the faster Auger recombination in the C/S QDs leads to partial decay of the QD population on the time scale of the instrument response function of our measurements (~200 ps), leading to the reduction of the apparent amplitude of the PL signal.

By extracting the fast decay component from the PL trace measured using a pump fluence just above the onset for the generation of multiexcitons ($<N>$ of ~0.1),[2, 26] we derive the biexciton lifetime τ_{XX} of 1.2±0.1 ns and 0.50±0.06 ns for the C/A/S (Figure 2c) and the C/S (Figure 2f) QDs, respectively. According to standard statistical scaling of radiative rates,[27, 29] the XX radiative lifetime ($\tau_{XX,r}$) is related to the measured single exciton radiative lifetime ($\tau_{x,r}$) by $\tau_{XX,r} = \tau_{x,r}/\beta$ with $\beta = 4$.[22, 30] Our analysis later in this work indicates that in the case of trion states in thick-shell CdSe/CdS QDs, β shows a slight deviation from the value of 2, predicated by statistical scaling. A recent study of ref. 31 suggests that in the case of biexcitons in core/shell CdSe/CdS QDs, β can also deviate from the "statistical value" of 4. However, according to this study, the deviation is not significant for shell thicknesses up to

13 CdS monolayers. In our samples, the shell is *ca*. 10 monolayers thick, suggesting the applicability of standard statistical arguments, which we use in our further analysis.

The biexciton Auger lifetime ($\tau_{XX,A}$) can be calculated from the overall lifetime using $1/\tau_{XX,A} = 1/\tau_{XX} - 1/\tau_{XX,r}$; this yields 1.5 ns and 0.54 ns for the C/A/S and C/S QDs, respectively (see Table 1). The suppression of Auger recombination in the C/A/S sample indicated by this analysis is the consequence of both a graded core/shell interface resulting in a "smoother" confinement potential as well as stronger delocalization of the exciton into the shell region. A longer Auger lifetime of the C/A/S QDs translates into the increased XX PL QY which is boosted to ~20.9% compared to ~6.9% for the C/S QDs (see Table 1).[22]

Dynamics of negative and positive trions. To study Auger recombination dynamics of charged multicarrier states we prepare negatively and positively charged QDs using photochemical doping. To inject extra electrons into QDs, we apply a recently-reported photochemical method, which makes use of lithium triethylborohydride (LBH) as a sacrificial hole scavenger (Scheme 1).[18] The addition of LBH (diluted in tetrahydrofuran and toluene; see Methods for details) to a deoxygenated QD toluene solution under inert atmosphere and exposure to room light caused a bleach of the 1S exciton absorption feature for both C/A/S (Figure 3a) and C/S (Figure 3d) QDs, which is indicative of electron injection into the conduction band. Further evidence for doping is provided by time-resolved PL measurements. As illustrated in Figure 3b&e, following the photodoping procedure, the PL decay becomes faster than in pristine, unexposed QDs, while the initial signal amplitude

increases. These observations are consistent with the presence of charged excitons that are characterized by higher rates of both radiative decay and Auger recombination compared to neural excitons.[14, 32, 33] The higher radiative rate leads to the increased PL amplitude accompanied by shortening of the PL dynamics, which is further accelerated due to nonradiative Auger recombination.

Exposure of charged QDs to air leads to almost immediate (within seconds) and complete recovery of the absorption spectrum, indicating that photochemical charging does not lead to any noticeable etching of the QD, which would have manifested in the blue shift of the 1S absorption peak.[19] However, the PL dynamics do not completely recover (Figure S1), likely due to partial degradation of the surface passivation leading to opening of surface-defect-related relaxation pathways.

To accurately extract the recombination dynamics of charged excitons and specifically account for the defect-related PL component, we compare the PL traces of charged QDs to those of not the pristine (unexposed) sample but the sample which was discharged by exposure to air; the “discharging” process, while removing the extra electrons from the QDs, leaves intact nonradiative channels introduced by photodoping chemistry. As illustrated in the insets of Figure 3b&e, the PL dynamics of charged QDs and recovered QDs can indeed be scaled such as to achieve a nearly perfect match of long-lived tails that are due to recombination of neutral excitons; in the case of photocharged samples, such excitons exist in the subset of dots remaining in the undoped state. The subtraction of the scaled PL traces removes the contribution from neutral species and yields dynamics due exclusively to

charged excitons. The measurements in Figure 3b&c correspond to low charging levels (the average per-dot electron number, $\langle n_e \rangle$, is ~0.2; see our discussion below), therefore, the extracted decay can be assigned to singly charged excitons or negative trions. The corresponding lifetimes (τ_{X-}) are 5.6 ns and 3.1 ns for the C/A/S and the C/S QDs, respectively (Table 1).

Next, we examined the possibility of QD charging with extra holes *via* a photochemical reaction. The key to success of photochemical doping is that after extracting the charge (an electron or a hole) from a QD, a charge-scavenging molecule should undergo an irreversible chemical reaction, which would prevent the transfer of the extracted charge back into the QD and hence ensure that QDs remain permanently charged. Thus, photochemical hole-doping requires an electron acceptor, which undergoes irreversible chemical changes upon scavenging a photogenerated electron from the QD (Scheme 1). The oxidizing agent selected for our studies is tris(*p*-bromophenyl)aminium hexachloroantimonate (TBHA; see its structure in Scheme 1), which is a well-known one-electron acceptor applied in organic and organometallic synthesis.[34-36] Once accepting an electron, TBHA is reduced from its radical form to the neutral tris(*p*-bromophenyl)amine which cannot be re-oxidized by the valence band hole from the QD.[37]

To initiate QD charging with extra holes, we add a TBHA solution in dichloromethane to a deoxygenated QD toluene solution under inert atmosphere and ambient illumination (see Methods for details). While this procedure does not cause any noticeable changes in the absorption spectra of either C/A/S (Figure 3a) or C/S (Figure 3d) QDs, it does not imply that

doping is unsuccessful. Indeed, as has been established by numerous transient absorption (TA) studies, the injected holes are not pronounced in TA spectra of II-VI QDs because the high spectral density of valence-band states leads to spreading of the hole population across multiple levels, which decreases single-state occupation factors and hence corresponding changes in absorption. [38] Based on these considerations, we apply transient PL measurements to detect the injected holes and quantify the dynamics of positively charged excitons.

To establish a neutral-sample reference for positively charged QDs, we reduce a QD solution, which was first treated with TBHA, by titrating it with LBH in the presence of ambient light (see Methods for details). In order to remove any access electrons from the QDs, which might have been generated due to overtreatment with LBH, we expose the titrated sample to air before spectroscopic measurements. As shown in Figure 3c&f, the titrated QDs exhibit slower decay and a lower initial amplitude than the original TBHA-treated sample. These trends are opposite to those observed for the LBH-treated pristine (*i.e.*, neutral) samples (Figure 3b), indicating that the TBHA exposure does lead to injection of holes into the QDs. The subtraction of the tail-normalized PL dynamics of the TBHA-treated sample and the same sample after its exposure to LBH (inset of Figure 3c) yields monoexponential decays for both the C/A/S (Figure 3c) and the C/S (Figure 3f) QDs, which we attribute to positive trion recombination; the corresponding lifetimes (τ_{X+}) are 3.3 ns and 1.5 ns (Table 1).

The conducted studies allow us to answer an interesting question on the sign of the QDs created *via* uncontrolled photocharging in the absence of any intentionally introduced redox species. This effect has been observed for many types of solution-based QD materials and has

been usually attributed to effects such as Auger-assisted ionization[33, 39, 40] and/or hot-carrier escape from the QD.[32, 41-43] In the case of CdSe-based QDs, photocharging has been usually assumed to produce negatively charged species,[21, 32, 33, 44] however, as indicated by single-dot measurements, it can also result in positively charged QDs.[17]

To investigate photocharging in the C/S and C/A/S QDs used in the present study, we compare PL dynamics of a QD solution measured using "static" and vigorously stirred samples, which has been a common approach to detect the presence of charged QDs and investigate dynamical and spectral signatures of charged excitons.[21, 41, 45] Due to a long lifetime of charge-separated species produced *via* photoionization, their abundance is increased in the case of a static *versus* a stirred solution, as in the latter case, the excitation volume is continuously replenished with fresh, charge-neutral QDs. Using this method, we find that lifetimes of trions produced by uncontrolled photoionization are 5.6 ns and 3.0 ns for the C/A/S and C/S QDs, respectively (Figure S2). These values are in close agreement with lifetimes of the X^- species in negatively charged QDs produced photochemically (Figure 3b&c). These observations indicate that the charged species primarily created by photoionization in our C/S and C/A/S samples are negative trions, which is consistent with the assignment made based on previous studies of similar core/shell samples.[21, 33]

Next, we compare the measured trion lifetimes to those of neutral biexcitons with the goal to verify the validity of the superposition principle (Equation 1), according to which the biexciton Auger decay can be described as occurring *via* two independent X^- and X^+ recombination channels. To extract Auger lifetimes of negative and positive trions ($\tau_{X^-,A}$ and

$\tau_{X+,A}$, respectively) from the measured time constants (Figure 3b,c,e,f), we use the following relationship, $1/\tau_{X-(X+),A} = 1/\tau_{X-(X+)} - 1/\tau_{X-(X+),r}$ where $\tau_{X-(X+),r}$ is the radiative lifetime of the negative (positive) trion. We further express trion radiative time constants as $\tau_{X-(X+),r} = \tau_{X,r}/\beta$, where β is the emission-rate enhancement factor of the trion state compared to the neutral exciton. In monocomponent QDs with mirror symmetric conduction and valence bands, $\beta = 2$.[12] However, recent studies of quasi-type-II CdSe/CdS QDs indicate that the repulsion between two delocalized electrons of the negative trion reduces β to below 2 values due to a reduced electron-hole overlap compared to the neutral exciton case. On the other hand, β is still close to 2 for the positive trion as both holes remain confined to the core region, as in the neutral exciton.[17, 30] Here we use $\beta = 1.5$ and 1.7 for the C/A/S and C/S QDs, respectively. These values are consistent with those from previous reports[17] and will be rigorously justified later based on measurements of QDs with a varied degree of charging.

Using the above considerations, we obtain that $\tau_{X-,A}$ and $\tau_{X+,A}$ are, respectively, 8.8 ns and 4.6 ns for the C/A/S QDs, and 3.8 ns and 1.7 ns for the C/S sample. Based on these values, the biexciton Auger lifetimes predicated by Equation 1 are 1.5 ns (C/A/S QDs) and 0.59 ns (C/S QDs). Both of these values are in perfect agreement with the results of direct optical measurements of XX dynamics according to which $\tau_{XX,A}$ = 1.5 ns and 0.54 ns for the C/A/S and the C/S QDs, respectively (Table 1). This analysis demonstrates that even in the case of strong asymmetry between the X^- and X^+ lifetimes, the Auger decay rate of a biexciton can still be calculated based on the superposition principle, *i.e.*, can be treated as resulting from superposition of two independent channels associated with positive and negative trion pathways. Furthermore, these results show that while affecting absolute values of Auger time

constants, the interface “smoothing” used for Auger-decay suppression does not affect the validity of the superposition principle. Therefore, a direct connection between $\tau_{XX,A}$ and $\tau_{X-(X+),A}$ lifetimes established by Equation 1 can be used to infer the Auger lifetime of trions of one sign based on the Auger lifetimes of the biexcitons and the trions of the opposite sign or, alternatively, to estimate the biexciton Auger lifetime based on the measured X^- and X^+ dynamics.

Carrier dynamics in QDs charged with multiple electrons. The methods of photochemical doping allow for injection of multiple charges into a QD. For example, as evident from the progressive bleaching of the 1S absorption peak, the exposure of the QDs to increasing amounts of LBH leads to the increasing number of electrons injected into QD quantized states (Figure 4a&b). The treatment with TBHA should also, in principle, allow for injecting multiple holes into the QDs. However, the exposure of the QDs to large amounts of TBHA leads to the degradation of their optically quality likely due to the distortion of the capping layer. Therefore, here we focus on effects associated with the injection of multiple electrons *via* photoreduction by LBH.

We extract recombination dynamics of charged excitons using the same procedure as in the previous subsection wherein we subtract tail-normalized PL traces of the charged and the re-neutralized samples (see examples in Figure 5a and 5b for the C/A/S and the C/S samples, respectively). As was mentioned previously, the long-time PL dynamics in charged samples are due to the subset of neutral QDs as following fast Auger recombination, all charged dots become nonemissive. Thus, the scaling factor used to match the post-Auger-decay PL tails of

charged and neutral QDs can be used to quantify the average number of extra-electron residing in the QDs. Specifically, if we assume that the probability of electron injection during photodoping follows the same Poisson statistics as the probability of photon absorption, then the fraction of uncharged QDs in the ensemble can be expressed as $q(0) = e^{-<n_e>}$.[13] Using this expression, we can obtain $<n_e>$ by assuming that $q(0)$ is equal to the scaling factor used in the "PL-tail-normalization" procedure. Based on this approach, we find that the absorption spectra of charged C/A/S QDs shown in Figure 4a correspond to $<n_e> =$ 0.5, 1, 1.7, and 6 (listed in the order of increasing 1S peak bleaching), while the spectra of the charged C/S QDs in Figure 4b correspond to $<n_e> = 1$ and 3. We further determine that for the data shown in Figure 3, $<n_e>$ is smaller than *ca.* 0.3, which indeed represents the weak charging limit when the prevailing charged photoexcited species are negative trions as was assumed in our earlier discussion. We would like to point out that the $<n_e>$ values obtained from the analysis of PL dynamics are consistent with those determined from the magnitude of the 1S absorption bleach (see Figure S3).

To quantify charged exciton lifetimes as a function of the number of extra electrons (τ_{n_e}), we fit the PL dynamics of a charged QD sub-ensemble (obtained by the subtraction procedure described above) using the following expression:

$$I_{ch}(t) = A_0 \sum_{n_e=1}^{\infty} \left[q(n_e) \beta e^{-t/\tau_{n_e}} \right] , \quad (2)$$

where A_0 is the early time PL peak amplitude of the re-neutralized QDs and $q(n_e)$ is the Poisson probability of a given QD to be occupied with n_e extra electrons. Here we assume that the radiative-rate enhancement factor β is the same for all charged excitons independent

on n_e because the 1S electron state monitored in our time-resolved PL measurements can accommodate no more than two electrons. Also, even in QDs charged with more than 2 electrons (n_e > 2), any of the Auger recombination events quenches PL as it necessarily removes the only hole present in the QD (in these measurements $\langle N_{ph} \rangle \ll 1$). Thus, even though our PL experiment monitors only the band-edge 1S transition, it is sensitive to all Auger recombination events including those involving the higher-energy 1P electrons. Therefore, these measurements provide accurate information on the overall lifetimes of all multiply-charged exciton states realized in our experiments.

By simultaneously fitting PL dynamics obtained for various values of $\langle n_e \rangle$ to Equation 2 with the same value of β (see Figure 5 and Figure S4), we obtain τ_{n_e} (n_e from 1 to 4) and β. Based on the best fits, β is 1.5 for the C/A/S QDs and 1.7 for the C/S samples; these values are close to those obtained from the analysis of single-dot PL dynamics for similar QD samples in ref. 17. While the exact reason underlying the difference in β between C/A/S and C/S QDs is not clear, it might indicate the increased disparity in the spatial distribution of the wave function of the second excited electron *versus* the first one in the case of the C/A/S QDs compared to the C/A/S particles. Using the derived values of τ_{n_e} and β, we next obtain the n_e-dependent Auger lifetimes of charged excitons ($\tau_{n_e,A}$) from $1/\tau_{n_e,A} = 1/\tau_{n_e} - 1/\tau_{n_e,r}$, where $\tau_{n_e,r} = \tau_{X,r}/\beta$. These lifetimes are displayed in Figure 5c and 5d (for the C/A/S and the C/S samples, respectively) as a function of n_e.

Next, we use these data to examine whether charged exciton lifetimes in II-VI QDs follow statistical scaling.[28, 46] Statistical scaling evolves from the superposition principle when the

rates of all elementary three-particle Auger events possible in a given multicarrier state are the same. As was discussed in the introduction, previous experimental studies have established the applicability of statistical scaling to Auger decay rates of both neutral and charged multiexciton states in PbSe QDs.[13, 28] However, PbSe is a unique semiconductor, which is characterized by mirror-symmetric conduction and valence bands and a high (eight-fold) degeneracy of the band-edge states.[27] These features lead to indistinguishable rates of elementary Auger events for all carriers comprising a given multicarrier state when N_e and N_h are ≤ 8,[12] which leads to the observed statistical scaling of Auger rates.

The situation, however, is more complicated in the case of II-VI QDs that are characterized by a considerable difference between conduction- and valence-band electronic structures. This breaks symmetry between the X^- and X^+ Auger decay channels leading to strongly different X^- and X^+ Auger lifetimes ($\tau_{X-,A} >> \tau_{X+,A}$), as discussed earlier. Furthermore, while the band edge hole state ($1S_{3/2}$) still has a fairly high four-fold degeneracy, the $1S_e$ band-edge electron level is only two-fold degenerate. Therefore, any multicarrier state with $N_e > 2$ necessarily contains a $1P_e$ electron, leading to the situation where the elementary Auger decay rates may become different for different carriers within the same multicarrier state. These specific features of II-VI materials might explain why Auger recombination rates observed for neutral multiexcitons in II-VI QDs do not follow statistical scaling,[2, 16] but instead are closer to a so-called “quantum-mechanical” scaling. [28, 46]

One might expect that the deviation from statistical scaling will be weaker for multiply negatively charged single-excitons than for neutral multiexcitons as in this case, intraband

Auger re-excitation involves only electrons, which excludes a source of asymmetry associated with the involvement of hole-related intra-band transitions. Further, multicarrier states are more forgiving than single-exciton states as concerns quantum-mechanical selection rules, which might diminish the difference in rates for individual Auger pathways involving $1S_e$ and $1P_e$ electrons. Indeed while in the case of single-exciton states, an inter-band transition involving the $1P_e$ electron and the $1S_{3/2}$ hole is strictly forbidden due to parity conservation, it becomes at least partially allowed in the presence of spectator charges in a multicarrier state because of mixing between closely separated $1S_{3/2}$ and $1P_{3/2}$ hole states, which can be ascribed to the effect of internal electric field.[47] The involvement of the asymmetric $1P_e$–$1S_{3/2}$ transition is necessary, for example, for explaining previous observations of bright emission due the $1P_e$ electron state and its fast radiative lifetimes in the case of states of fairly low multiplicity (*e.g.*, tri-excitons and negatively charged biexcitons) when the $1P_{3/2}$ hole state is still unoccupied.[29,48] Furthermore, in our own measurements, we also observe 1P emission in heavily charged QDs despite using a sub-single-exciton excitation regime, when the only excited hole resides in the $1S_{3/2}$ state leaving the $1P_{3/2}$ state unpopulated (Figure S5). All of these observations suggest that the rates of elementary Auger event for the $1S_e$ and $1P_e$ electrons might be comparable, which would result in statistical scaling of overall Auger decay rates for multiply charged single-exciton states.

Under single-exciton excitation condition, the electron and hole occupancies of a photoexcited QD containing n_e extra electrons are $N_e = n_e + 1$ and $N_h = 1$. If we further assume that all elementary Auger events have identical rates, then the overall Auger lifetime of the exciton in the presence of n_e extra electrons can be presented as

$$\tau_{n_e,A} = (r_{0,A})^{-1}\left[(n_e+1)n_e\right]^{-1} \quad . \qquad (3)$$

Using Equation 3 with $r_{0,A}$ as an adjustable parameter, we can indeed closely reproduce time constants $\tau_{n_e,A}$ derived from experimental measurements (blue symbols in Figure 5c&d; blue lines are based on Equation 3). These results suggest that the rates of elementary Auger event involving 1S and 1P electrons are indeed not significantly different, which results in the observed statistical scaling. Based on the fits, the characteristic time constant per individual Auger pathway ($\tau_{0,A} = 1/r_{0,A}$) is 17.4 ns and 7.5 ns for the C/A/S and the C/S QDs, respectively.

We further use the Auger and radiative lifetimes of multiply-charged excitons to find their "ideal" PL QYs calculated by accounting for intrinsic Auger decay but neglecting all other extrinsic channels for nonradiative recombination (Figure 5f). We obtain that negative-trion QYs are ~36% and ~18% for the C/A/S and the C/S QDs, respectively. Since Auger lifetimes scale faster with increasing n_e than radiative lifetimes, the PL QY progressively decreases with increasing n_e, and in the case of four extra electrons it drops to ~5% and ~2%, for the C/A/S and the C/S QDs, respectively.

Conclusions

To summarize, we have prepared both positively and negatively charged CdSe/CdS core/shell QDs using photochemical doping. We use the doped QDs to quantify radiative and Auger lifetimes of positively and negatively charged excitons and to infer the scaling of Auger decay rates with the number of extra carriers. Additionally, we evaluate the influence of the shape of the interfacial profile ("sharp" *versus* "smooth") on the absolute values of Auger

time constants as well as their dependence on the number of extra carriers. The analysis of the experimental data indicates that the Auger lifetimes of both neutral and charged multicarrier states can be accurately described by the superposition principle according to which Auger decay of a given multicarrier state can be considered in terms of a superposition of independent "elementary" three-particle recombination events. Specifically, we demonstrate that the biexciton Auger recombination rates can be presented as twice the sum of the negative- and positive-trion Auger decay rates. Furthermore, using multiply-negatively-charged QDs, we observe that in this case, the Auger decay rates exhibit statistical scaling [$\propto n_e(n_e + 1)$] up to maximum doping levels ($n_e = 4$) used in the measurements. Since the multi-carrier states with $n_e > 1$ contain both $1S_e$ and $1P_e$ electrons, this result suggests that the rates of individual Auger pathways do not strongly depend on the exact type of a quantum-mechanical state occupied by the electron involved in Auger recombination. Further, we observe that while incorporation of a graded alloy layer at the core/shell interface does affect (suppresses) Auger rates for both negative and positive trions, it does not lead to violation of the superposition principle. These results suggest that this principle is likely general to quantum-confined nanocrystals, and therefore, can be used as a predictive tool for evaluating Auger lifetimes of various multicarrier states in nanocrystals of arbitrary compositions and complexities.

Methods/Experimental

Materials. Cadmium oxide (CdO, 99.999%), trioctylphosphine (TOP, 97%), elemental sulfur (S, 99.999%) and elemental selenium (Se, 99.999%) were purchased from Strem Chemicals. Oleylamine (70%), oleic acid (OA, 90%), 1-octadecene (ODE, 90%), 1-

dodecanethiol (DDT, 98%), dichloromethane, toluene, Lithium triethylborohydride (LBH, 1 M solution in THF), and tris(*p*-bromophenyl)aminium hexachloroantimonate (TBHA) were purchased from Sigma-Aldrich. All chemicals were used without further processing.

Synthesis of CdSe/CdS and CdSe/CdSe$_x$S$_{1-x}$/CdS QDs. To prepare CdSe/CdS core/shell QDs, we adopted a modified version of the synthetic procedure by Bae *et al*,[21] using DDT as a sulfur source. Briefly, CdSe cores (C) with the mean radius of 1.5 nm, fabricated *via* a literature method by Yang *et al*,[49] were purified several times and dispersed in hexane. To grow a CdS shell, 0.7 μmol of CdSe cores and 20 mL of ODE were placed in a flask and degassed at 120 ºC for 20 min. After back-filling with N_2, 0.6 mL of 0.5 M $Cd(OA)_2$ (heating 10 mmol of CdO, 10 mL of oleic acid, and 10 mL ODE at 200 ºC) and 0.6 mL of 0.5 M DDT (diluted in ODE) were added into the flask and reacted at 300 ºC for 60 min. Then, 6.5 mL of 0.5M $Cd(OA)_2$ and 6.5 mL of 0.5 M DDT were slowly added to the flask with the 1 mL/hr of injection rate.

For the synthesis of core/alloy (C/A) CdSe/CdSe$_x$S$_{1-x}$ QDs, 0.5 M TOPSe (dissolving 3 mmol of selenium powder in 1.5 mL of TOP and 4.5 mL of ODE) was chosen as a selenium source. At 300 ºC, a mixture of TOPSe and DDT (x mL of 0.5 M SeTOP, y mL of 0.5 M DDT, and 2 mL of ODE) was continuously injected to a flask containing 0.7 μmol of CdSe cores, 1.4 mL of 0.5 M $Cd(OA)_2$, and 20 mL ODE. To control Se content in the alloyed layer, the precursor ratio (x mL/y mL) and the injection rate were varied as follows: 2.25/0.75 and 1.6 mL/hr for 18 min; 1.5/1.5 and 1.4 mL/hr for 35 min; 0.75/2.25 and 1.2 mL/hr for 60 min. To deposit a CdS shell onto C/A QDs and generate a C/A/S structure, 6 mL of 0.5M $Cd(OA)_2$ and 6 mL of 0.5 M DDT were slowly injected to the flask with the 1 mL/hr injection rate. At

the end of the reaction, the fabricated QDs were purified several times by a standard precipitation/re-dispersion procedure using hexane and ethanol. Finally, the QDs were dispersed in toluene for photochemical charging experiment.

QD doping with electrons. LBH (1 M solution in THF) was diluted to 0.01 M using toluene for photochemical electron doping experiments. CdSe/CdS QDs dissolved in toluene were loaded into custom-made airtight cuvettes (optical path 1 mm). The sample optical density at the band-edge 1S peak was <0.1. To mitigate surface etching of the QDs in the charging experiments, ~10 mg of extra TOPO and ~0.5 mL of TOP were added to a 4 mL QD solution. The QD solution was brought into an N_2- filled glove box (oxygen level <0.1 ppm) and shielded from illumination until charging. For the charging experiment, typically 100-1000 equivalents of LBH per CdSe/CdS QDs were used. These amounts are considerably higher than those used in previous reports on doping of CdSe QDs (10-100 equivalents),[18] which can be explained by the fact that hole scavenging from the thick-shell CdSe/CdS QDs is more challenging than in the case of core-only or thin-shell samples. Typically, we used ambient room light to initiate photochemical charging, and within several minutes we were able to reach a steady charged state. We found that additional illumination with a 405-nm light emitting diode (LED; ~2 mW/cm^2 power density) accelerated this process. The number of extra electrons introduced per QD could be controlled by the amount of added LBH and was monitored by UV-vis absorption.

QD doping with holes. 80 mg of TBHA was dissolved in 10 mL dichloromethane to make a 0.01 M solution for photochemical hole-doping experiments. The CdSe/CdS QDs dissolved in toluene were loaded the same type of optical airtight cuvettes as in electron-

dopig experiments. The hole doping was also performed in the N_2 atmosphere (oxygen level <0.1 ppm). Typically, ~1000 equivalents of TBHA per CdSe/CdS QDs were used. To minimize deleterious side reactions of TBHA with QD surface ligands we increase the relative rate of photo-doping, by applying 405 nm LED illumination (~2 mW/cm^2 power density). Because the reaction between TBHA and ligands introduces nonradiative surface trapping sites, the TBHA treated QDs showed faster PL decay than QDs treated with LBH (see Figure 3 of the main text). To remove the extra holes from the QDs (*i.e.*, discharge QDs), we used LBH to titrate the TBHA-treated QDs. The amount of LBH (in terms of the number of molecules) used was *ca.* twice that of the TBHA molecules to ensure complete discharging of the QDs. To remove any extra electrons generated by exposure to LBH, the titrated solution was then exposed to air.

Conflict of Interest

The authors declare no competing financial interest.

Supporting Information Available

Figures S1-S5 contain measurements of PL dynamics in negatively charged QDs following their exposure to air, measurements of trion dynamics in QDs charged *via* photoionization, modeling of absorption bleaching in charged QD ensembles, recombination dynamics of excitons in the presence of multiple extra-electrons, and observations of 1P emission in heavily negatively charged QDs. This material is available free of charge *via* the Internet at http://pubs.acs.org.

Acknowledgements

V.I.K. was supported by the Chemical Sciences, Biosciences and Geosciences Division, Office of Basic Energy Sciences, Office of Science, U.S. Department of Energy. J.L. and K. W. acknowledge support by the Laboratory Directed Research and Development program at Los Alamos National Laboratory.

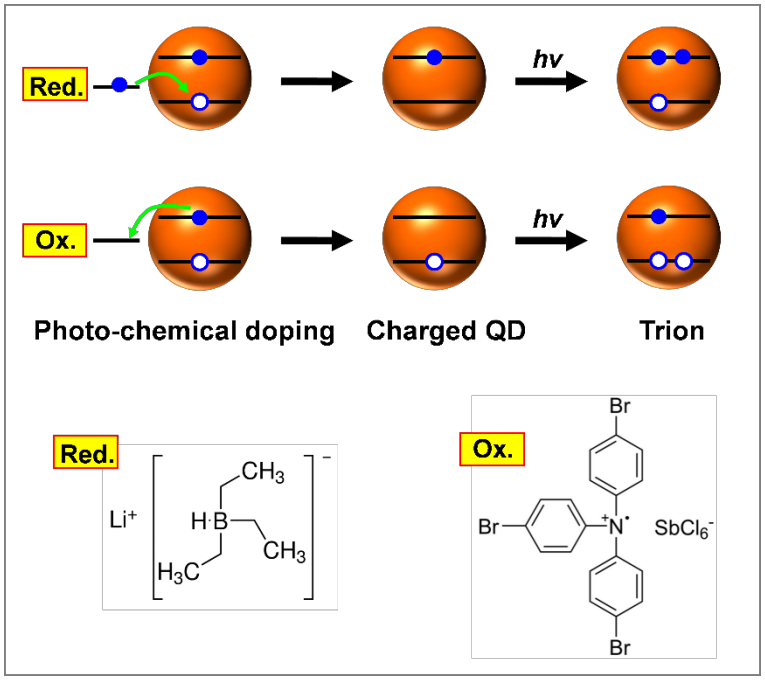

Scheme 1. Negatively and positively charged QDs by photo-chemical doping. Top: to create a negatively charged QD, a reducing reagent (Red.) is used to scavenge the photo-generated hole from the QD, leaving behind an excess electron in the conduction band of the QD. Photo-excitation of this QD leads to a negatively charged exciton or a so-called negative trion. Middle: to create a positively charged QD, an oxidizing reagent (Ox.) is used to scavenge the photo-generated electron from the QD, leaving behind an excess hole in the QD valence band. Photo-excitation of this QD leads to a positively charged exciton or a positive trion. Bottom: the chemical structures of lithium triethylborohydride (LBH, left) and tris(*p*-bromophenyl)aminium hexachloroantimonate (TBHA, right) that are used as the reducing and oxidizing agents, respectively. Both of these molecules undergo irreversible reactions after being oxidized or reduced, rendering QDs permanently charged.

Table 1. Lifetimes and "ideal" emission quantum yields (QYs) of single-exciton and various multi-carrier states in C/A/S and C/S QDs

	C/A/S QD				C/S QD			
	X	**XX**	**X^-**	**X^+**	**X**	**XX**	**X^-**	**X^+**
τ_{tot}[a] (ns)	23	1.2	5.6	3.3	29	0.5	3.1	1.5
τ_r[b] (ns)	23	5.75	15.3	11.5	29	7.25	17.0	14.5
τ_A[c] (ns)	NA	1.5	8.8	4.6	NA	0.54	3.8	1.7
QY[d] (%)	100	20.9	36.5	28.7	100	6.9	18.2	10.3

(a) Total lifetime; (b) Radiative lifetime; (c) Auger lifetime; (d) "Ideal" emission QYs are calculated based on the radiative and Auger lifetimes and neglecting all non-Auger-related nonradiative processes.

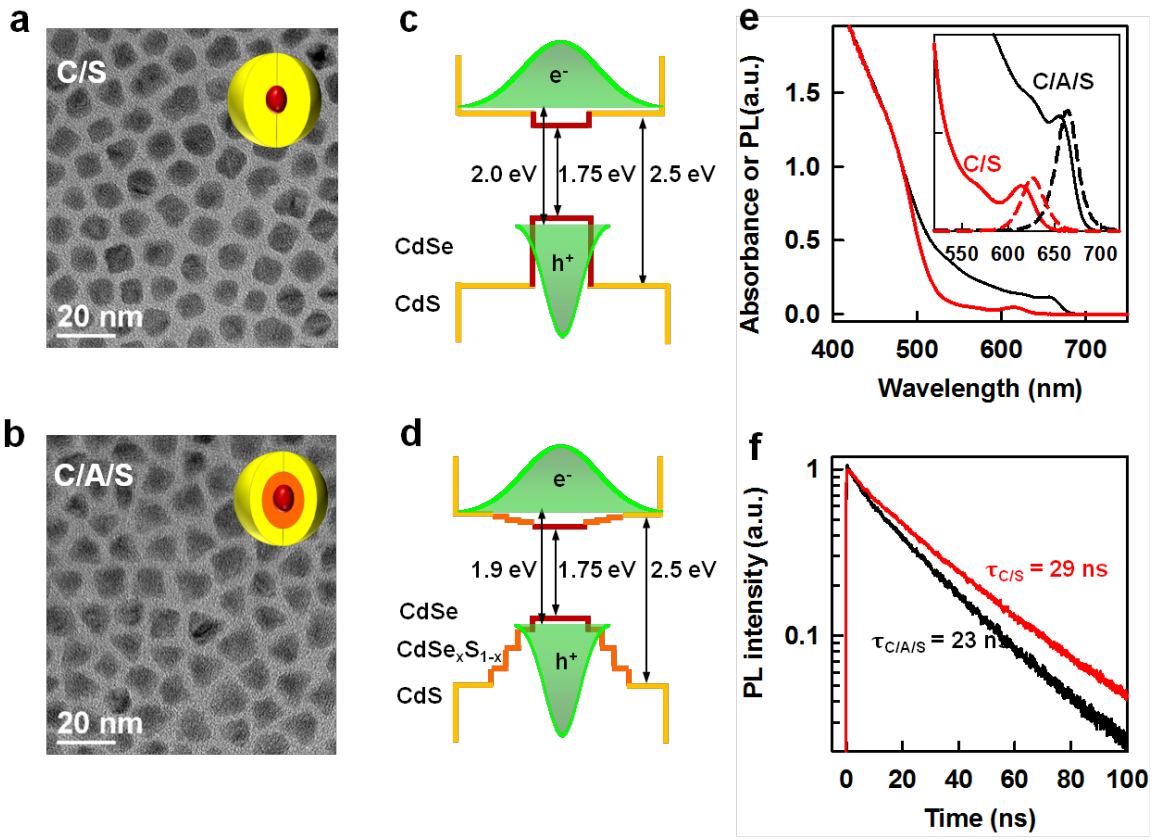

Figure 1. Core/shell (C/S) and core/alloy/shell (C/A/S) QDs. (a&b) Representative transmission electron microscopy (TEM) images of CdSe/CdS core /shell (C/S) QDs **(a)** and CdSe/$CdSe_xS_{1-x}$/CdS core/alloy/shell (C/A/S) QDs **(b)**. The core diameter is 3 nm for both QDs and the total diameters are 9.4 and 9.2 nm for the C/A/S and the C/S QDs, respectively. **(c&d)** Schematic band structures of the C /S **(c)** and the C/A/S **(d)** QDs. C/A/S has a three-step, graded layer between core and shell while C/S has a sharp core/shell interface. **(e)** Absorption spectra of the C/A/S (black) and the C/S (red) QDs. Inset is an expanded view of the band-edge (core-related) absorption spectra and photoluminescence (PL) spectra. **(f)** Time-resolved PL dynamics of the C/A/S (black) and the C/S (red) QDs recorded using low-intensity excitation (sub-single-exciton regime) at 3.1 eV.

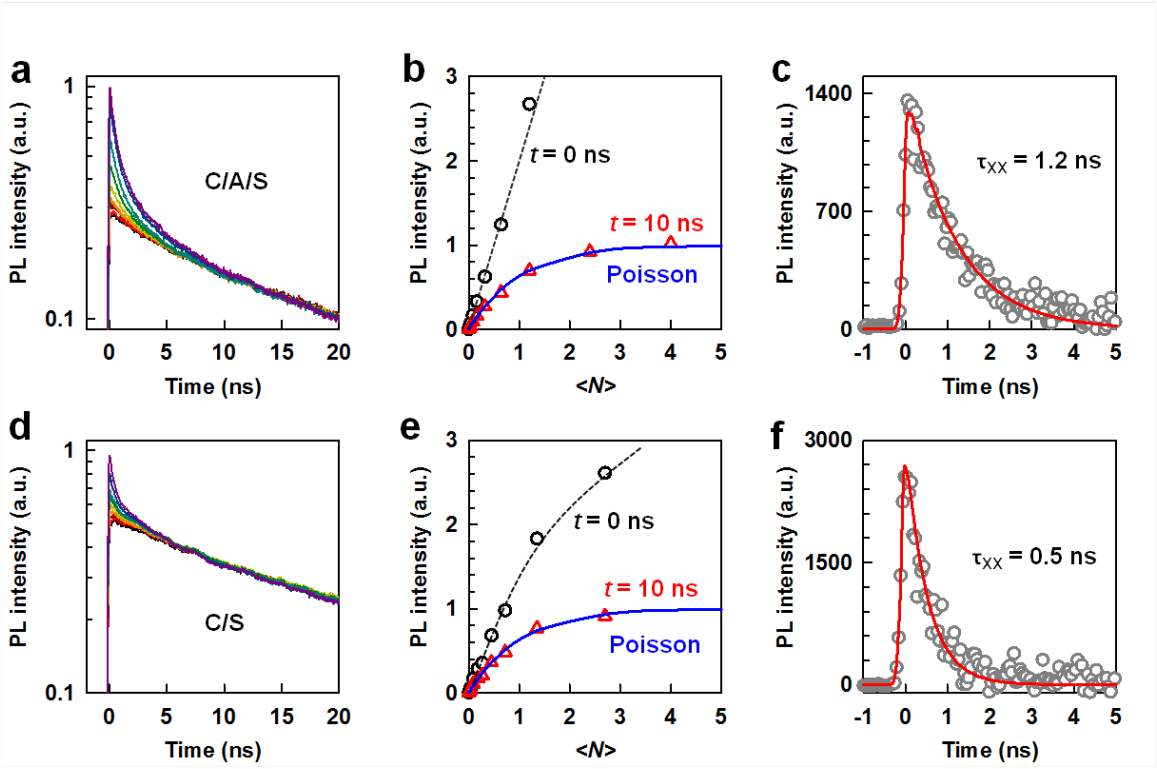

Figure 2. Excitation-fluence dependent PL dynamics in C/A/S (a-c) and C/S (d-f) QDs. (a&d) PL dynamics monitored at the PL peak as a function of excitation fluence for the C/A/S **(a)** and the C/S **(d)** QDs. Pump photon energy is 3.1 eV and the per-pulse pump fluence is varied from a few nJ/cm^2 to 1000s of nJ/cm^2; corresponding initial average QD excitonic occupancies (<*N*>) are from 0.002 to 5. Traces are normalized at *t* = 10 ns. **(b&e)** PL intensity at indicated times as a function of <*N*> for the C/A/S **(b)** and the C/S **(e)** QDs. For both samples, the PL intensities at 10 ns (red triangles) saturates according to Poissonian statistics (blue lines). The *t* = 0 PL intensity (black circles) shows a linear growth for the C/A/S QDs, and a sublinear increase for the C/S QDs. Black lines are a guide to the eye. **(c&f)** Biexciton recombination dynamics (gray circles) for the C/A/S **(c)** and the C/S **(f)** QDs obtained by subtracting PL traces corresponding to <*N*>=0.2 and 0.1. The red solid lines are single exponential fits convoluted with the instrument response function (~0.2 ns width).

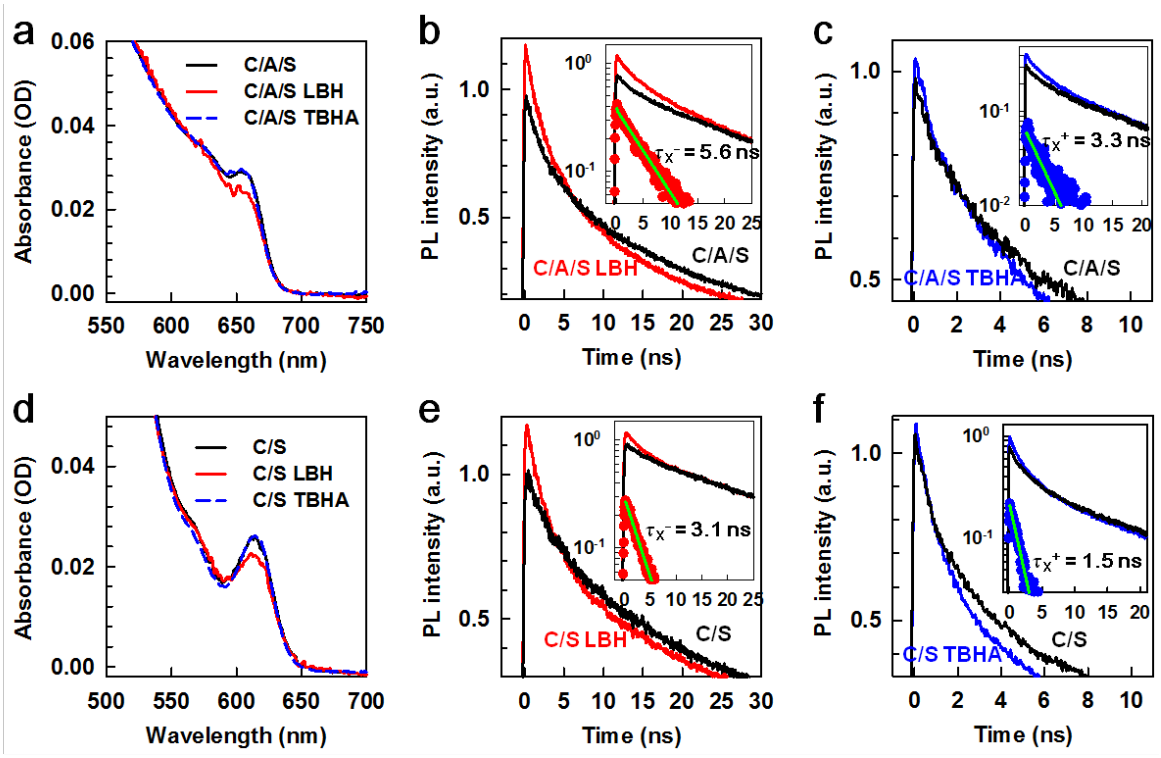

Figure 3. Absorption spectra and PL dynamics of charged C/A/S (a-c) and C/S (d-f) QDs. (a&d) Absorption spectra of neutral (black solid line), negatively charged (red solid line), and positively charged (blue dashed line) C/A/S **(a)** and C/S **(d)** QDs. **(b&e)** Time-resolved PL dynamics of neutral (black line) and negatively charged (LBH-treated, red line) C/A/S **(b)** and C/S **(e)** QDs recorded using low-intensity ($<N_{ph}> <<1$), 3.1 eV excitation. The neutral-QD dynamics are obtained by exposing the LBH-treated QDs to air. Insets are PL dynamics scaled such as to match the long-lived tails. The subtraction of tail-normalized PL dynamics reveals negative-trion decay (red circles). The green lines are single-exponential fits to the negative trion dynamics. **(c&f)** Time-resolved PL dynamics of neutral (black line) and positively charged (TBHA-treated, blue line) C/A/S **(c)** and C/S **(f)** QDs recorded using low-intensity ($<N_{ph}> <<1$), 3.1 eV excitation. The neutral QD dynamics are obtained by titrating the TBHA-treated QDs with LBH and then exposing them to air to remove extra electrons. Insets are PL dynamics scaled such as to match the long-lived tails. The subtraction of tail-normalized PL dynamics reveals positive-trion decay (blue circles). The green lines are single-exponential fits to the positive trion dynamics.

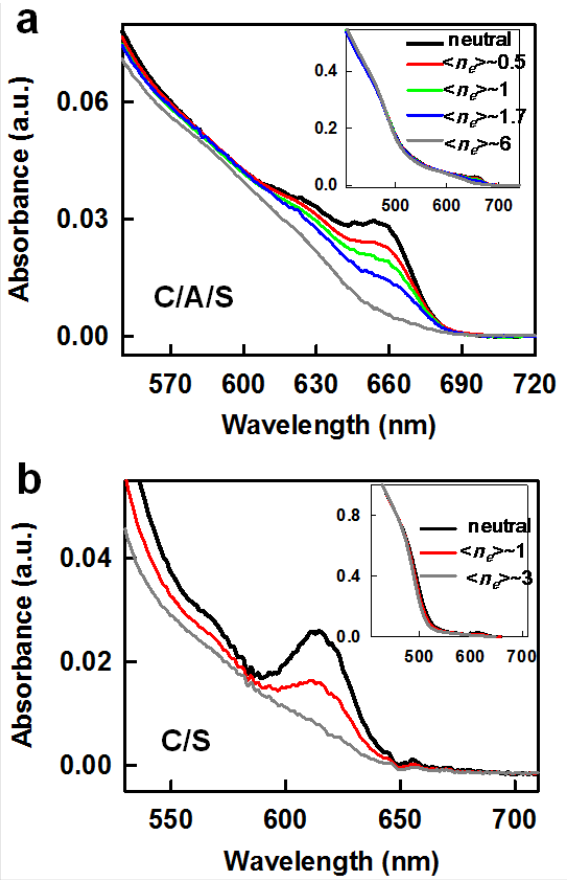

Figure 4. Absorption spectra of C/A/S and C/S QDs charged with multiple electrons. (a) C/A/S QDs with the average number of extra electrons per QD (<n_e>) of 0 (black), 0.5 (red), 1.0 (green), 1.7 (blue), and 6 (gray). **(b)** Absorption spectra of C/S QDs for <n_e> = 0 (black), 1.0 (red), and 3.0 (gray). The insets in **a** and **b** show the same absorption spectra but over an extended wavelength range. The fact that the absorption spectra remain unchanged at high spectral energies (corresponding wavelengths <500 nm) indicates that the effects of QD etching during photochemical doping are negligible.

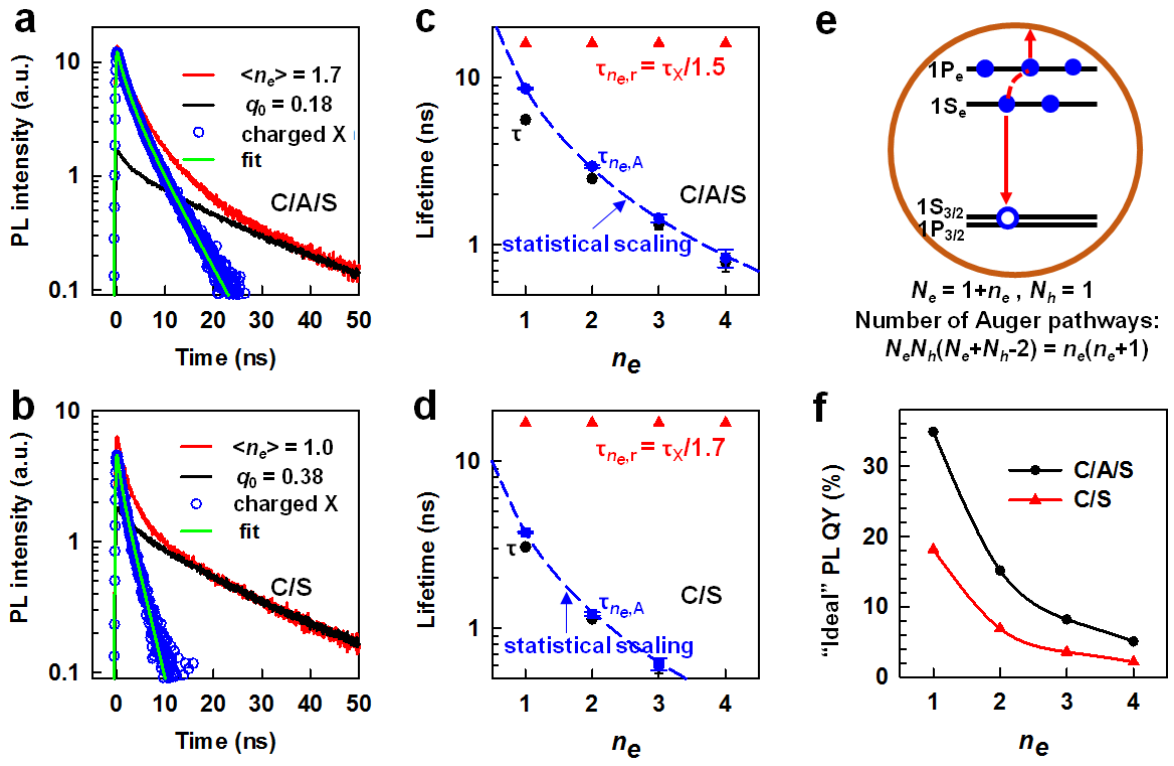

Figure 5. Scaling of Auger lifetimes with the number of extra electrons. (a&b) PL dynamics of the C/A/S QDs with <n_e> of ~1.7 **(a)** and the C/S QDs with <n_e>of ~1 **(b)**. The red and black solid lines are PL dynamics of charged and "discharged" (by exposure to air) QDs, respectively. The latter are scaled such as to match the long-lived tail of the charged QDs trace (the scaling factors, q_0, are indicted in the legends). A subtraction of these two traces generates dynamics, which is solely due to charged excitons (blue circles; denoted as "Charged X"). The green lines are fits according to the model described by Equation 2. **(c&d)** Charged exciton lifetime (τ_{n_e}, black circles) as a function of the number of extra electrons (n_e) in the C/A/S **(c)** and the C/S **(d)** QDs. Using overall (τ_{n_e}) and radiative ($\tau_{n_e,r}$ red triangles) lifetimes, we obtain Auger lifetimes ($\tau_{n_e,A}$, blue squares). The blue dashed line is calculated assuming statistical scaling of the $\tau_{n_e,A}$ values. **(e)** Schematic illustration of an elementary Auger event wherein recombination of the $1S_e$ electron and the $1S_{3/2}$ hole is accompanied by intraband re-excitation of the $1P_e$ electron. According to statistical scaling arguments, the number of all possible interband transitions is given by N_eN_h and the number of all possible energy transfer pathways can be presented as (N_e+N_h-2). In the case of negatively charged excitons, $N_e = 1 + n_e$ and $N_h = 1$. This yields the following scaling law for the Auger rate: $1/\tau_{n_e,A} \propto n_e(1 + n_e)$. **(f)** "Ideal" PL QYs of negatively charged excitons as a function of n_e for the C/A/S (black) and the C/S (red) QDs; in these calculations we neglect all non-Auger-decay related nonradiative processes.

References

1. Landsberg, P. T., *Recombination in Semiconductors*. Cambridge University Press: **2003**.
2. Klimov, V. I.; Mikhailovsky, A. A.; McBranch, D. W.; Leatherdale, C. A.; Bawendi, M. G., Quantization of Multiparticle Auger Rates in Semiconductor Quantum Dots. *Science* **2000**, *287*, 1011-1013.
3. Robel, I.; Gresback, R.; Kortshagen, U.; Schaller, R. D.; Klimov, V. I., Universal Size-Dependent Trend in Auger Recombination in Direct-Gap and Indirect-Gap Semiconductor Nanocrystals. *Phys. Rev. Lett.* **2009**, *102*, 177404.
4. Pandey, A.; Guyot-Sionnest, P., Multicarrier Recombination in Colloidal Quantum Dots. *J. Chem. Phys.* **2007**, *127*, 111104.
5. Fisher, B.; Caruge, J.-M.; Chan, Y.-T.; Halpert, J.; Bawendi, M. G., Multiexciton Fluorescence from Semiconductor Nanocrystals. *Chem. Phys.* **2005**, *318*, 71-81.
6. Pietryga, J. M.; Park, Y.-S.; Lim, J.; Fidler, A. F.; Bae, W. K.; Brovelli, S.; Klimov, V. I., Spectroscopic and Device Aspects of Nanocrystal Quantum Dots. *Chem. Rev.* **2016**, *116*, 10513-10622.
7. Klimov, V. I.; Mikhailovsky, A. A.; Xu, S.; Malko, A.; Hollingsworth, J. A.; Leatherdale, C. A.; Eisler, H. J.; Bawendi, M. G., Optical Gain and Stimulated Emission in Nanocrystal Quantum Dots. *Science* **2000**, *290*, 314-317.
8. Fan, F.; Voznyy, O.; Sabatini, R. P.; Bicanic, K. T.; Adachi, M. M.; McBride, J. R.; Reid, K. R.; Park, Y.-S.; Li, X.; Jain, A.; Quintero-Bermudez, R.; Saravanapavanantham, M.; Liu, M.; Korkusinski, M.; Hawrylak, P.; Klimov, V. I.; Rosenthal, S. J.; Hoogland, S.; Sargent, E. H., Continuous-Wave Lasing in Colloidal Quantum Dot Solids Enabled by Facet-Selective Epitaxy. *Nature* **2017**, *544*, 75-79.
9. Park, Y.-S.; Bae, W. K.; Baker, T.; Lim, J.; Klimov, V. I., Effect of Auger Recombination on Lasing in Heterostructured Quantum Dots with Engineered Core/Shell Interfaces. *Nano Lett.* **2015**, *15*, 7319-7328.
10. Bae, W. K.; Park, Y.-S.; Lim, J.; Lee, D.; Padilha, L. A.; McDaniel, H.; Robel, I.; Lee, C.; Pietryga, J. M.; Klimov, V. I., Controlling the Influence of Auger Recombination on the Performance of Quantum-Dot Light-Emitting Diodes. *Nat. Commun.* **2013**, *4*, 2661.
11. Bae, W. K.; Brovelli, S.; Klimov, V. I., Spectroscopic Insights into the Performance of Quantum Dot Light-Emitting Diodes. *MRS Bull.* **2013**, *38*, 721-730.
12. Klimov, V. I., Multicarrier Interactions in Semiconductor Nanocrystals in Relation to the Phenomena of Auger Recombination and Carrier Multiplication. *Annu. Rev. Condens. Matter Phys.* **2014**, *5*, 285-316.
13. Koh, W.-k.; Koposov, A. Y.; Stewart, J. T.; Pal, B. N.; Robel, I.; Pietryga, J. M.; Klimov, V. I., Heavily Doped n-Type PbSe and PbS Nanocrystals Using Ground-State Charge Transfer from Cobaltocene. *Sci. Rep.* **2013**, *3*, 2004.
14. Jha, P. P.; Guyot-Sionnest, P., Trion Decay in Colloidal Quantum Dots. *ACS Nano* **2009**, *3*, 1011-1015.
15. Cohn, A. W.; Rinehart, J. D.; Schimpf, A. M.; Weaver, A. L.; Gamelin, D. R., Size Dependence of Negative Trion Auger Recombination in Photodoped Cdse Nanocrystals. *Nano Lett.* **2014**, *14*, 353-358.
16. Padilha, L. A.; Bae, W. K.; Klimov, V. I.; Pietryga, J. M.; Schaller, R. D., Response of Semiconductor Nanocrystals to Extremely Energetic Excitation. *Nano Lett.* **2013**, *13*, 925-932.
17. Park, Y.-S.; Bae, W. K.; Pietryga, J. M.; Klimov, V. I., Auger Recombination of Biexcitons and Negative and Positive Trions in Individual Quantum Dots. *ACS Nano* **2014**, *8*, 7288-7296.
18. Rinehart, J. D.; Schimpf, A. M.; Weaver, A. L.; Cohn, A. W.; Gamelin, D. R., Photochemical Electronic Doping of Colloidal Cdse Nanocrystals. *J. Am. Chem. Soc.* **2013**, *135*, 18782-18785.
19. Shim, M.; Guyot-Sionnest, P., n-Type Colloidal Semiconductor Nanocrystals. *Nature* **2000**, *407*, 981-983.
20. Qin, W.; Guyot-Sionnest, P., Evidence for the Role of Holes in Blinking: Negative and Oxidized CdSe/CdS

Dots. *ACS Nano* **2012**, *6*, 9125-9132.
21. Bae, W. K.; Padilha, L. A.; Park, Y.-S.; McDaniel, H.; Robel, I.; Pietryga, J. M.; Klimov, V. I., Controlled Alloying of the Core–Shell Interface in CdSe/CdS Quantum Dots for Suppression of Auger Recombination. *ACS Nano* **2013**, *7*, 3411-3419.
22. Park, Y.-S.; Bae, W. K.; Padilha, L. A.; Pietryga, J. M.; Klimov, V. I., Effect of the Core/Shell Interface on Auger Recombination Evaluated by Single-Quantum-Dot Spectroscopy. *Nano Lett.* **2014**, *14*, 396-402.
23. Cragg, G. E.; Efros, A. L., Suppression of Auger Processes in Confined Structures. *Nano Lett.* **2009**, *10*, 313-317.
24. Climente, J. I.; Movilla, J. L.; Planelles, J., Auger Recombination Suppression in Nanocrystals with Asymmetric Electron–Hole Confinement. *Small* **2012**, *8*, 754-759.
25. García-Santamaría, F.; Brovelli, S.; Viswanatha, R.; Hollingsworth, J. A.; Htoon, H.; Crooker, S. A.; Klimov, V. I., Breakdown of Volume Scaling in Auger Recombination in CdSe/CdS Heteronanocrystals: The Role of the Core−Shell Interface. *Nano Lett.* **2011**, 11, 687-693.
26. Garcia-Santamaria, F.; Chen, Y. F.; Vela, J.; Schaller, R. D.; Hollingsworth, J. A.; Klimov, V. I., Suppressed Auger Recombination in "Giant" Nanocrystals Boosts Optical Gain Performance. *Nano Lett.* **2009**, *9*, 3482-3488.
27. McGuire, J. A.; Sykora, M.; Joo, J.; Pietryga, J. M.; Klimov, V. I., Apparent *Versus* True Carrier Multiplication Yields in Semiconductor Nanocrystals. *Nano Lett.* **2010**, *10*, 2049-2057.
28. Klimov, V. I.; McGuire, J. A.; Schaller, R. D.; Rupasov, V. I., Scaling of Multiexciton Lifetimes in Semiconductor Nanocrystals. *Phys. Rev. B* **2008**, *77*, 195324.
29. Park, Y. S.; Malko, A. V.; Vela, J.; Chen, Y.; Ghosh, Y.; García-Santamaría, F.; Hollingsworth, J. A.; Klimov, V. I.; Htoon, H., Near-Unity Quantum Yields of Biexciton Emission from CdSe/CdS Nanocrystals Measured Using Single-Particle Spectroscopy. *Phys. Rev. Lett.* **2011**, *106*, 187401.
30. Sampat, S.; Karan, N. S.; Guo, T.; Htoon, H.; Hollingsworth, J. A.; Malko, A. V., Multistate Blinking and Scaling of Recombination Rates in Individual Silica-Coated CdSe/CdS Nanocrystals. *ACS Photonics* **2015**, *2*, 1505-1512.
31. Hiroshige, N.; Ihara, T.; Saruyama, M.; Teranishi, T.; Kanemitsu, Y., Coulomb-Enhanced Radiative Recombination of Biexcitons in Single Giant-Shell CdSe/CdS Core/Shell Nanocrystals. *J. Phys. Chem. Lett.* **2017**, *8*, 1961-1966.
32. Galland, C.; Ghosh, Y.; Steinbruck, A.; Sykora, M.; Hollingsworth, J. A.; Klimov, V. I.; Htoon, H., Two Types of Luminescence Blinking Revealed by Spectroelectrochemistry of Single Quantum Dots. *Nature* **2011**, *479*, 203-207.
33. Galland, C.; Ghosh, Y.; Steinbrück, A.; Hollingsworth, J. A.; Htoon, H.; Klimov, V. I., Lifetime Blinking in Nonblinking Nanocrystal Quantum Dots. *Nat. Commun.* **2012**, *3*, 908.
34. Bell, F. A.; Ledwith, A.; Sherrington, D. C., Cation-Radicals: Tris-(*p*-Bromophenyl)Amminium Perchlorate and Hexachloroantimonate. *J. Chem. Soc. C* **1969**, 2719-2720.
35. Connelly, N. G.; Geiger, W. E., Chemical Redox Agents for Organometallic Chemistry. *Chem. Rev.* **1996**, *96*, 877-910.
36. Rinehart, J. D.; Weaver, A. L.; Gamelin, D. R., Redox Brightening of Colloidal Semiconductor Nanocrystals Using Molecular Reductants. *J. Am. Chem. Soc.* **2012**, *134*, 16175-16177.
37. Osovsky, R.; Cheskis, D.; Kloper, V.; Sashchiuk, A.; Kroner, M.; Lifshitz, E., Continuous-Wave Pumping of Multiexciton Bands in the Photoluminescence Spectrum of a Single CdTe-CdSe Core-Shell Colloidal Quantum Dot. *Phys. Rev. Lett.* **2009**, *102*, 197401.
38. Klimov, V. I., Optical Nonlinearities and Ultrafast Carrier Dynamics in Semiconductor Nanocrystals. *J. Phys. Chem. B* **2000**, *104*, 6112-6123.

39. Peterson, J. J.; Nesbitt, D. J., Modified Power Law Behavior in Quantum Dot Blinking: A Novel Role for Biexcitons and Auger Ionization. *Nano Lett.* **2009**, *9*, 338-345.
40. Klimov, V. I.; McBranch, D. W., Auger-Process-Induced Charge Separation in Semiconductor Nanocrystals. *Phys. Rev. B* **1997**, *55*, 13173-13179.
41. McGuire, J. A.; Sykora, M.; Robel, I.; Padilha, L. A.; Joo, J.; Pietryga, J. M.; Klimov, V. I., Spectroscopic Signatures of Photocharging Due to Hot-Carrier Transfer in Solutions of Semiconductor Nanocrystals under Low-Intensity Ultraviolet Excitation. *ACS Nano* **2010**, *4*, 6087-6097.
42. Padilha, L. A.; Robel, I.; Lee, D. C.; Nagpal, P.; Pietryga, J. M.; Klimov, V. I., Spectral Dependence of Nanocrystal Photoionization Probability: The Role of Hot-Carrier Transfer. *ACS Nano* **2011**, *5*, 5045-5055.
43. Krauss, T. D.; O'Brien, S.; Brus, L. E., Charge and Photoionization Properties of Single Semiconductor Nanocrystals. *J. Phys. Chem. B* **2001**, *105*, 1725-1733.
44. Javaux, C.; Mahler, B.; Dubertret, B.; Shabaev, A.; Rodina, A. V.; Efros, A. L.; Yakovlev, D. R.; Liu, F.; Bayer, M.; Camps, G.; Biadala, L.; Buil, S.; X., Q.; Hermier, J. P., Thermal Activation of Non-Radiative Auger Recombination in Charged Colloidal Nanocrystals. *Nat. Nanotechnol.* **2013**, *8*, 206-212.
45. McGuire, J. A.; Joo, J.; Pietryga, J. M.; Schaller, R. D.; Klimov, V. I., New Aspects of Carrier Multiplication in Semiconductor Nanocrystals. *Acc. Chem. Res.* **2008**, *41*, 1810-1819.
46. Klimov, V. I., Multicarrier Interactions in Semiconductor Nanocrystals in Relation to the Phenomena of Auger Recombination and Carrier Multiplication. *Annu. Rev. Condens. Matter Phys.* **2014**, *5*, 285-316.
47. Diaconescu, B.; Padilha, L. A.; Nagpal, P.; Swartzentruber, B. S.; Klimov, V. I., Measurement of Electronic States of PbS Nanocrystal Quantum Dots Using Scanning Tunneling Spectroscopy: The Role of Parity Selection Rules in Optical Absorption. *Phys. Rev. Lett.* **2013**, *110*, 127406.
48. Fisher, B.; Caruge, J. M.; Zehnder, D.; Bawendi, M., Room-Temperature Ordered Photon Emission from Multiexciton States in Single CdSe Core-Shell Nanocrystals. *Phys. Rev. Lett.* **2005**, *94*, 087403.
49. Yang, Y. A.; Wu, H.; Williams, K. R.; Cao, Y. C., Synthesis of CdSe and CdTe Nanocrystals without Precursor Injection. *Angew. Chem. Int. Ed.* **2005**, *44*, 6712-6715.